Forecasting Research

Forecasting Research Division
Scientific Paper No. 32

TOWARDS IMPROVED RADAR ESTIMATES OF SURFACE PRECIPITATION RATE AT LONG RANGE

by

M. Kitchen

March 1995

Meteorological Office
London Road
Bracknell
Berkshire
RG12 2SZ
United Kingdom

Forecasting Research Division
Scientific Paper No. 32

TOWARDS IMPROVED RADAR ESTIMATES OF SURFACE PRECIPITATION RATE AT LONG RANGE

by

M. Kitchen

March 1995

TOWARDS IMPROVED RADAR ESTIMATES OF SURFACE PRECIPITATION RATE AT LONG RANGE.

M Kitchen
Meteorological Office, Bracknell, Berks, UK

Abstract

A method of estimating surface precipitation rates from radar data at several beam elevations has been developed. An idealized reflectivity factor profile is constructed at each pixel with the profile defined in terms of three unknowns; the 'background' reflectivity factor and the slope of the reflectivity factor profile in two layers above the freezing level. Assumptions of horizontal homogeneity in the profile shape are necessary, but are only invoked above the freezing level. Simple parametrizations of low-level orographic growth and the bright band are used, and the profile diagnosis is assisted by the use of meteorological information other than from radar. The difference between the idealized profiles and the observations is expressed as a penalty which is minimised by iteration, thus avoiding complicated inversion methods. In a simulation experiment, the method proved particularly successful in reducing errors due to the bright band. At long range, the use of radar data from several elevations was found to be beneficial in reducing bias errors in most cases. Tests using real radar data confirmed that in conditions where the reflectivity profile shape deviated markedly from the norm, the scheme was able to avoid the application of unrepresentative and detrimental long range corrections which would result from an assumption of a climatalogical profile shape above the freezing level. However, in typical frontal rainfall, the method showed no consistent improvement over a simpler method using data from a single elevation angle. Unresolved spatial variability in the reflectivity factor profile remains a problem.

1. INTRODUCTION

Correction of radar data from ranges where the lowest elevation beam is above the freezing level is extemely difficult because of the enormous variability in the shape of relectivity profile within the ice. The variability arises on a wide range of scales down to that of individual radar pixels (Kitchen and Jackson, 1993). In a recent study of weather radar performance, Fabry *et al* (1992) concluded that beyond the range where the radar horizon intercepts the freezing level, 'any attempt to obtain quantitative rainfall estimates is futile. Furthermore, this range is a maximum useful range for all scanning strategies.....'. Unfortunately, the spacing of the radars in the UK network is such that over most of the land area, the lowest radar beam is centred more than 1 km above sea level and, for 5% of the area, the beam centre is at more than 3 km altitude. As the freezing level is commonly below 1km in the winter, these 'long range' corrections must be attempted if complete radar coverage is to be maintained. Kitchen *et al* (1994), hereafter referred to as KBD, described a radar correction scheme in which observational data, combined with simple parametrizations of the bright band and low-level orographic growth, were used to construct an idealized reflectivity factor profile at each pixel. One weakness of their method was that, between the freezing level and the observed cloud top, a climatalogical profile shape was assumed. This gave acceptable results in cases of widespread frontal precipitation similar to those for which the climatology was derived, but was susceptible to large bias errors at long

range if the profile deviates significantly from that assumed. There was also the problem that the top of the precipitation layer is sometimes much lower than the observed cloud top height with the result that the radar beam starts to overshoot the precipitation at shorter ranges than anticipated.

The overall objective of the work described here was to try and improve the performance of the KBD correction scheme at long range by using radar data from several beam elevations to assist in the diagnosis of the reflectivity profile. Almost all radars in the UK network scan at 4 different elevation angles from 0.5 deg up to 2.5 or 4 deg, with the data output as averages over 5km pixels. At present, only data from the lowest elevation beam is routinely transmitted. However, from 1995, data from all beams should be available centrally in real-time. Use of these upper beams in a correction scheme was first proposed by Harrold and Kitchingman (1975). The shape of the vertical profile of reflectivity factor was to be derived directly from the ratio between measurements at just two elevations by inversion of the equations that provide the ratio. Their inversion method was criticized by Carpenter (1983), who proposed an alternative. Neither scheme was developed for operational use. The method of Smith (1984) was somewhat similar, in that data from two different elevations was used to correct for the bright band only. The theory was simpler than in the Carpenter scheme and it was implemented operationally for a time. More recently Koistinen (1991) and Gray (1991) have developed methods, for use in Finland and New Zealand respectively, in which an average reflectivity factor profile is derived from all available beams close to the radar. The average profile is then used to calculate corrections which are applied to data from longer ranges. Andrieu *et al* (1995) have also recently proposed a new inversion method for retrieving the profile.

A potential problem with these methods is that assumptions of spatial homogeneity in profile shape are required in the derivation of the profile and/or in the application of the corrections to data over a wide area. In contrast, the bright band height, intensity and the magnitude of any orographic growth cause related variations in the profile shape on small scales. Smith (1990) suggested that the most effective correction methods would be those which could resolve as much as possible of this variability, and this is the reasoning behind the pixel-by-pixel parametrizations adopted by KBD. However, methods similar to those of Koistinen and Gray offer advantages at long range because they avoid the assumption of a climatalogical average ice profile shape. Thus it was considered advantageous to try and combine the best features of both approaches.

In the new method, radar data from all ranges are used in a consistent manner, but most information on the shape of the profile above the freezing level is obtained from pixels where several radar beams intercept precipitation in this region. This is typically at short to moderate radar ranges in winter. Unfortunately, the information is of value at long range where the lowest elevation beam is above the freezing level. Thus, if we are to avoid extrapolation in the vertical, some assumption of horizontal homogeneity is necessary, at least above the freezing level. The simplest approach is to assume that some variable parameters which define the shape of the idealized profile within the ice are constant over the radar image. Thus, at the outset, the inability to resolve variability in the ice profile shape on small scales was recognised and the realistic aim was to avoid detrimental long range corrections on the scale of the radar domain.

The single variable parameter used to define the idealized reflectivity profile in the KBD method was the reflectivity factor in the rain beneath the melting layer in each pixel. This was varied iteratively to reconcile the measurement of reflectivity in the lowest elevation beam with a value calculated from the idealized profile. In the present development, the measurements from a number of beam elevations are utilized to slightly increase the number of profile variables which describe the shape of the reflectivity factor profile above the freezing level. Complicated inversion methods of solution are avoided by expressing the difference between the idealized profile and the radar measurements as a penalty function which is minimised by iteration. The

new method is referred to subsequently as the multiple-beam method and it is described in more detail in section 2. Initial testing of the method was in a simulation experiment described in Section 3. In section 4, the results of a limited verification using operational radar data are presented. Finally, some conclusions and ideas for further development are noted in section 5.

2. THE MULTIPLE-BEAM METHOD

(a) The idealized reflectivity profile.

The idealized reflectivity factor profile is illustrated in Fig 1. Below the freezing level, the parametrizations for the bright band and orographic growth are similar to those used by KBD. The turning points in the profile are defined by the following expressions.

Let the reflectivity factor and the precipitation rate at the ground be denoted by Z_s and R_s respectively. Z_b is the 'background' reflectivity factor in the rain just beneath the melting layer. The orographic enhancement, O, expressed as a rainfall rate, is taken to be an additive correction and is estimated from a consideration of low level winds and humidity, see Hill (1983). A standard $Z - R$ relationship of the form $Z = A\,R^{\mu}$ is assumed.

$$R_s = \left(\frac{Z_b}{A}\right)^{1/\mu} + O \tag{1}$$

$$Z_s = A\left(\left(\frac{Z_b}{A}\right)^{1/\mu} + O\right)^{\mu} \tag{2}$$

Any orographic growth is assumed to be linear in Z and to commence at a height of Δh_O (= 1.5 km) above the ground.

Figure 7 in Davies (1992) shows a scatter plot of values of the area of the bright band peak, B, in units of $\mathrm{mm^6 m^{-2}}$ and Z_b in $\mathrm{mm^6 m^{-3}}$ on logarithmic scales. A straight line fitted by eye through these data provides the relationship;

$$\log B = 1.42 \log Z_b + 2.1 \tag{3}$$

In the idealized profile, the bright band is assumed to be a isosceles triangle of depth Δh_B and area given by equation 3. The peak reflectivity in the idealized profile, Z_B, is then given by;

$$Z_B = Z_b + \frac{252\, Z_b^{1.42}}{\Delta h_B} \tag{4}$$

Δh_B was taken to be 500 m.

Estimates of height of the freezing level h_{FL} in each pixel are provided by a mesoscale numerical forecast model that has a horizontal resolution of 17.5 km.

Examination of reflectivity profiles suggests that they commonly follow an approximately exponential decay of reflectivity factor with height (equivalent to a linear decrease in reflectivity expressed in dBZ). In the present method, the reflectivity factor above h_{FL}, is assumed to grow or decay exponentially with height in two layers up to the cloud top height, h_t, where it is assumed to fall to zero.

$$Z(h) = Z_j\, e^{a_{j'}(h - h_j)} \tag{5}$$

where $a_{j'}$ is a constant within the two layers in the profile above the freezing level (numbers 5 and 6, see Fig 1). The subscript j is used to denote the level in the idealized profile and j'

is the corresponding profile layer above level j. The depth of the layer immediately above the freezing level was chosen to be 2km. This layer thickness is comparable to the radar beam width at all except extreme range so there is the realistic expectation that the radar data is capable of resolving gradients on this scale. For Z in units of $mm^6\ m^{-3}$, $a_{j'} = -1.0\ km^{-1}$ is equivalent to a slope of -4.343 dB km^{-1}. The reflectivity factor at the freezing level is assumed to be Z_b.

Thus, the Z profile at each pixel is specified in terms of three unknowns, Z_b, which varies from pixel to pixel; a_5 and a_6, which are uniform over the radar image.

The potential of this idealized profile to resolve variations above the freezing level was first examined by analysing measured reflectivity profiles. These were constructed from RHI (Range Height Indication) scans recorded by the Chilbolton radar operated by the Rutherford Appleton Laboratory. The profile dataset was the same as that described in Kitchen and Jackson (1993). Those profiles where the maximum in reflectivity (assumed to be associated with the bright band) in the range 1.0 - 2.5 km were selected for further analysis. The lower height limit was necessary to be able to estimate the reflectivity in the rain beneath the melting layer (the background reflectivity factor); the upper limit ensured that there was sufficient data from above the freezing level for the analysis. The profile slope in a layer $\approx$ 2 km deep above the freezing level (i.e. $\approx a_5$) was estimated, based upon the same assumptions as used to construct the idealized reflectivity factor profile. The freezing level was taken to be 250 m above the level of maximum reflectivity and a straight line was fitted to the reflectivity factors (expressed in dBZ_e) in the layer 350 - 2350 m above the freezing level. The line was constrained to pass through the freezing level at the background value of the reflectivity factor. Fig 2 shows this construction schematically. The slopes of the fitted lines for those profiles in the period Jan - Mar 1988 are plotted as a series in Fig 3. Note that this is not strictly a time series since the data are not continuous. However, to provide some sort of time scale for the x-axis, a continuous series would provide about 45 profiles per hour. This series is typical of the whole dataset (3 years in total) and shows that for much of the time, the point-to-point scatter in a_5 was almost as large as the total range of values. In these conditions, the assumption of horizontal homogeneity is flawed and the idealized profile will not be representative. However, the series also exhibits periods (e.g. profile numbers 230-270 and 350-380)when a_5 deviated systematically from the mean value and a correct determination of a_5 should result in reduced bias errors in surface precipitation rate at long range.

(b) The penalty function.

The form of the penalty function was arrived at after some experimentation.

$$J = \sum_i \sum_n \frac{1}{(n+1)^2} \log^2 \left(\frac{(Z_c + \epsilon)}{(Z_m + \epsilon)} \right) \tag{6}$$

where J is the penalty for a given radar image and is a sum over all 'wet' pixels in the image, i, and over all available radar beams in those pixels, n. The different beams are denoted 0 to 3; n=0 being the lowest elevation beam. Z_c is the calculated reflectivity factor that the radar beam n would measure in pixel i given the idealized reflectivity factor profile in that pixel. Z_m is the corresponding measured reflectivity factor. ϵ is a constant (in reflectivity units).

The reasons behind the particular formulation of J are as follows:-

- Z_c and Z_m range over 5 orders of magnitude so the use of $\log Z$ in the expression reduces the range of J and assists in the iterative solution. The log ratio is squared so that J has a minimum when all $Z_c = Z_m$.

- Most information on the surface precipitation rate is provided by beam 0, particularly where it is beneath the freezing level. The preferred solution is one in which the fit of the idealized reflectivity profile to the beam 0 measurement is closer than for the other beams. The $1/(n+1)^2$ term reduces the relative weight given to upper beam data but is not intended to reflect any difference in the measurement errors.

- The constant ϵ fulfils two purposes. It is necessary to avoid numerical problems when $Z_c = 0$; which arises when the whole depth of a radar beam is entirely above h_t. Secondly, precipitation detected by the lowest elevation beam may be undetected by one or more upper beams. In these pixels, the upper beam data are providing some information, but it is limited because it is unknown as to whether the signal is identically zero or just below the minimum detectable signal (MDS). If, in all such cases, the true signal is assumed to be zero, then in situations where the true signal is closer to the MDS, the result could be an unrealistically large negative value of $a_{j'}$. ϵ has the effect of downweighting the contribution to the total penalty from pixels and beams where the measurment is close to or less than ϵ compared to those where the signal is larger. The choice of ϵ needs to reflect the MDS for a particular radar and the probability that, given a zero measurement, the true signal is zero. In practice, a change in ϵ of an order of magnitude results in a small, but significant change in the slopes a_5 and a_6. This formulation is not ideal, and a more formal treatment of errors in both the radar data and the profile parametrizations would be preferable (see also section 5).

If there are N wet pixels in a beam 0 radar image, there are $N+2$ unknowns and up to $4N$ measurements. However, a large fraction of the upper beam data are typically zeroes and so the number of data providing unambiguous information are usually much less than $4N$. The large dimensions of the penalty minimisation problem places restrictions on the choice of the functional form of both the idealized profile and the beam power profile (see later). The following simple function was fitted to the two-way beam power profile;

$$P(\phi) = \frac{\cos(k\phi) + 1}{2} \tag{7}$$

where k is a constant =225 and ϕ is the off-axis beam angle in radians. The function is valid for values of ϕ in the range -0.014 to 0.014. This function provides a good fit to the power profile measured by the radar manufacturers for $\phi < 0.006$ rad, whereas it underestimates the power transmitted at angles > 0.010 rad (see Fig 4). The differences are considered to be insignificant in view of the uncertainty of about 0.002 rad in the true beam elevation.

The solution also requires that the vertical coordinate in the idealized reflectivity factor profiles is ϕ rather than height, h.

$$h = h_{radar} + \frac{r^2}{1.33 \,.\, 2R_0} + r\sin(\gamma + \phi) \tag{8}$$

where h_{radar} is the height of the radar antenna above sea level, r is the radar range, R_0 is the radius of the earth, γ is the beam elevation angle. The factor of 1.33 is the usual empirical correction for the effect of refraction. For the operational radars in the UK network, $\gamma \leq 0.070$ rads. Also we are only interested in layers in the idealised reflectivity profile which are intersected by the radar beam. These are typically a few kilometres deep so for ranges greater than order 25km, relevant values of ϕ are less than 0.2 rads. The maximum error arising from the approximation $\sin(\gamma + \phi) \simeq (\gamma + \phi)$ is therefore $\simeq 0.003$ rads and can be ignored as being similar to the uncertainties in beam elevation mentioned above. Thus we have:-

$$\phi = (h - h_{radar} - \frac{r^2}{1.33\,.\,2r_0} - r\gamma) \tag{9}$$

At very short radar ranges (<25km), the approximation may effectively distort the idealized profile where there are large gradients in reflectivity factor in the vertical. However, at these ranges, the radar beams are commonly within rain beneath the freezing level where gradients (and corrections) are relatively small. Above the freezing level, for small γ and ϕ (see above), $h - h_{j'} \simeq r(\phi - \phi_{j'})$ and we can rewrite equation 5 as;

$$Z(\phi) \simeq Z_j \, e^{a_{j'} r(\phi - \phi_j)} \tag{10}$$

(c) Minimization of the penalty.

As a first guess, Z_b was set equal to Z_m as measured by the lowest elevation beam, a_5 and a_6 were set equal to a typical average value of -1.4.

Z_c is calculated for an individual pixel and radar beam by weighting the idealized reflectivity factor profile by the beam power profile.

$$Z_c = \sum_{j'} \frac{\int_\alpha^\beta Z(\phi)\, P(\phi)\, d\phi}{\int_\alpha^\beta P(\phi)\, d\phi} \tag{11}$$

where the sum is over all the layers in the profile, j', which are intersected by the radar beam. The limits α and β are either the boundaries of the profile layer or of the radar beam. The integration is in one dimension only whereas strictly, the integration should be over the two dimensional beam power profile. However, for a Gaussian profile, the results of the integration will be the same. The differences between the function fitted to the beam power and a Gaussian are small compared to the uncertainty in elevation angle (see Fig 4) and the simplification is adequate for this purpose.

Minimization of the penalty function was accomplished using standard NAg [1] routine E04DGE which is suitable for large scale problems. No bounds can be placed on the variables during the iteration but Z_b was limited to a reflectivity factor equivalent to a maximum of $10 \times R_m$ (Z_m expressed as an equivalent rainfall rate) for output. To improve the scaling of the problem, $\log Z_b$ rather than Z_b is the variable used in the minimization routine. When applied to operational radar data, with up to a few thousand wet pixels in an image, no more than 10 iterations are normally sufficient to locate the minimum to within a small tolerance. The NAg routine requires expressions to be provided not only for J but also its gradient with respect to the unknowns, $\partial J/\partial \log Z_b$ (N values), $\partial J/\partial a_5$ and $\partial J/\partial a_6$. The form of the beam power profile and the idealized reflectivity factor profile were chosen in the knowledge that analytic expressions for these quantities would be needed. As J is a simple function of Z_c, the task is essentially that of deriving expressions for Z_c, $\partial Z_c/\partial Z_b$, $\partial Z_c/\partial a_5$ and $\partial Z_c/\partial a_6$. Some key steps involved in their calculation are provided in an appendix. Once solutions for Z_b, a_5 and a_6 are found, R_s is obtained from equation 1.

The computer time required to correct a radar image is similar to that required by the KBD scheme, despite the much higher volume of data. This is due to the efficiency of the NAg routine and the avoidance of numerical integration.

[1] The Numerical Algorithms Group Limited

3. EVALUATION USING SYNTHETIC RADAR DATA

A simulation method was adopted for initial testing so as to to minimise the impact of measurement and sampling errors on the results.

Operational radar measurements were synthesized from Chilbolton radar reflectivity factor profile dataset as described in Kitchen and Jackson (1993). Twelve periods of an hour were selected during which the freezing level was below 2.5km (to provide an adequate test at long range) and there was negligible orographic enhancement (for simplicity). The periods were also chosen to provide a range of profile shapes above the freezing level. The average profiles for each period are plotted in Fig 5.

The operational radar was assumed to be at a height of 100m and to have a horizon at 0.0 deg elevation. Data for three beams at 0.5, 1.0 and 1.5 deg. elevation were synthesized. The maximum radar range within the UK radar network is 210km, so from each profile, radar measured rainfall rates (R_m) at 8 different ranges (25,50,75.... 200km) were calculated. At ranges up to 100km, the MDS was taken to be 7.2 mm^6m^{-3}; increasing with the square of the range beyond 100 km. This corresponds to a conservative estimate of the operational radars detection capability (Kitchen and Jackson, 1993). If R_m was calculated to be less than the MDS then R_m was set to zero. An hour long time series of Chilbolton profiles contained about 50 profiles and thus radar data for about 400 pixels were created. These pixels were assumed to form the 'wet' pixels in a single instantaneous operational radar image. The Chilbolton profiles were examined to estimate a typical height of the freezing level which was then assumed to be constant over the image. In reality, variations in the freezing level height were observed during the hour long periods but the magnitude of the variations was no larger than the uncertainty in estimating the height on an operational basis ($\approx$ 200 m). h_t was taken to be the typical maximum height for which the Chilbolton radar detected precipitation during each period. The true surface precipitation rate, R_T was estimated from the Chilbolton reflectivity measurements at a height of 500m above sea level assuming the same $Z - R$ relationship as in the correction scheme.

The multiple-beam method was used to produce estimates of surface precipitation rate (R_s) from the synthesized image. Initial tests indicated a reasonable choice for ϵ was 1.0 mm^6m^{-3}. The final penalty per pixel (J/N) was between $\approx$ 0.01 and 0.05 which was typically about an order of magnitude smaller than the initial penalty.

The comparisons between R_s and R_T were grouped according to the radar range. To act as control and to measure the impact of the data from higher elevation beams, a simpler correction method was also applied to the synthetic data. This used the same bright band parametrization, but only radar data from the lowest beam were processed. Layer 6 was dropped and layer 5 extended up to h_t. a_5 was set to a typical climatalogical value of -1.4 km^{-1} $\equiv$ -6 $dBkm^{-1}$. Thus, the control method was very similar to the KBD scheme.

In Fig 6, $\overline{(R_s - R_T)}$ is plotted as a function of radar range both for the control and multiple-beam methods. $\overline{(R_m - R_T)}$ is also plotted for comparison. The mean differences at ranges of 75 and 200 km are also listed in Table 1. The corrections applied at long range by the multiple-beam method are largely determined by a_5, so the values are listed in this table. The results for ranges where the radar beam is mainly below the freezing level are very similar for both multiple-beam and control methods. The bright band parametrization was mainly successful in reducing bias errors at short and moderate range. The multiple-beam scheme reduced the mean error at the range of the bright band peak in all but one case (10 Apr 1989). The mean absolute bias at 75km range was reduced by 80% compared to the raw data and the mean RMS error was reduced by 64%.

In some of the cases, the reflectivity factor only decreased slowly with height above the freezing level. For example, in the 19th Nov 1987 case, only very small range corrections were

required even at extreme range. Assumption of a fixed profile slope caused the control method to overestimate surface precipitation rates by more than a factor of two on average. The 13 Jan 1988 (0200-0300UTC), 28 Sep 1988 and 10 Apr 1989 cases are other examples of over-correction at long range by the control method.

The precipitation layer in the 12th Jan case was very shallow, with no measurable reflectivity recorded above about 2.5 km, which was only about 800 m above the freezing level. The very rapid fall off in reflectivity so close to the freezing level caused the control method to underestimate the correction required. Similarly, in the following hour (13 Jan 1988 0000-0100UTC, the long range bias error was very large with $\overline{\log(R_m/R_T)} = -1.26$ at 200km range, i.e. the required correction was about a factor of 20 on average. This means that the limitation on the background precipitation rate to no more than 10 times R_m will have significantly restricted the ability of the corrections to remove the bias. Nevertheless, the scheme produced a worthwhile reduction in both the bias and RMS errors at long range.

Two failures for the multiple-beam method were the 23 Sep 1988 and the 12 Apr 1989 cases. They were probably due to large variations in the Chilbolton profile shape during the hour. Some failures are to be expected given the scatter in Fig 3 and the assumption of horizontal homogeneity in the method. Problems may also be expected when the error in the height of the freezing level is large compared to the depth of the melting layer. The large gradients in the vertical profile of reflectivity factor associated with the bright band are then mis-intepreted as being associated with the profile slope above the freezing level. Despite these failures, over these twelve cases, the mean absolute bias error at 200km range from the multiple-beam method was 64% lower than that for the raw radar data and 35% lower than for the control method.

The final penalty per pixel (J/N) is a measure of the fit of the idealized reflectivity factor profiles to the radar data. Fig 7 is a plot of RMS $\log(R_s/R_T)$ against (J/N). The correlation suggests that the penalty per pixel may be a predictor of the error in surface precipitation rate estimates and may have a useful quality control function (see section 5).

Harris (1977) noted that a common observation in RHI scans recorded by sensitive radars is of ice precipitation generated in moist layers which completely evaporates in dry layers beneath. In these conditions, the application of climatalogically-based long range corrections will produce a gross overestimate of the precipitation reaching the surface. By defining two layers above the freezing level, the correction scheme has the potential for diagnosing total or partial evaporation of ice, if it is sufficiently widespread.

Two such cases of widespread evaporation were identified in the Chilbolton dataset and three, hour-long periods were selected from these cases. The average profiles of reflectivity factor are plotted in Fig 8. In the first case (14th Oct 1987 1700-1800UTC), very light snow (max reflectivity factor = 5 $\mathrm{dbZ_e}$) evaporated at around 5 km altitude. Below 2.5 km, very rapid growth commenced and the average reflectivity factor beneath the melting layer was about 21 dBZ. The multiple-beam method produced estimates of a_5 and a_6 of -4.4 and 2.6 $\mathrm{km^{-1}}$ respectively; reflecting the rapid growth above the melting layer and the elevated precipitation layer above. Unfortunately, the profile parametrization seriously overestimated the intensity of the bright band in this case and the corrections were relatively ineffective (Fig 9). A much better result was achieved in the 15th Oct 1987 (1000-1100UTC) case where a deep layer of moderate snow evaporated completely just above the freezing level at around 2 km. a_5 and a_6 were estimated to be 2.2 and -2.7 $\mathrm{km^{-1}}$, very close to the values estimated directly from the average reflectivity factor profile in Fig 8. The corrections reduced the estimated mean surface precipitation rate to less than 0.1 $\mathrm{mmh^{-1}}$,from a measured mean equivalent rate of about 0.5 $\mathrm{mmh^{-1}}$. At 200km range, the control method overestimated the average surface rate at 2.8 $\mathrm{mmh^{-1}}$. Note that, as the variable in the multiple-beam method iteration is the log of the background reflectivity factor, it is impossible for the estimated surface precipitation rate to

be reduced to identically zero. During the following hour (15th Oct 1987 1100-1200UTC), an increasing proportion of the precipitation reached the surface, and by the end of the period, there was little evidence of evaporation. The scheme produced values of a_5 and a_6 of 0.4 and -3.4 km^{-1}, which again provided much better corrections at long range than the control (Fig 9).

The results of the simulation experiment represent an indication of the performance of the correction scheme in near-ideal circumstances. They suggest potential for improved long-range corrections in some cases, notably for widespread evaporation. However, cases where the radar data are degraded must be expected, given that we are unable to properly resolve all significant profile shape variations. Some tests on real radar data were performed to support these conclusions.

4. EVALUATION OF THE METHOD APPLIED TO OPERATIONAL RADAR DATA

The multiple-beam method was tested in a total of 11 cases which are listed in Table 2. The first 4 cases were selected because climatalogically-based long range corrections in the KBD method produced poor results for at least part of the time, so there was scope for the multiple-beam method to provide improved corrections. Fig 10 shows time series of a_5 produced by the multiple-beam correction scheme applied to operational radar data from these 4 cases. Point-to point scatter was confined to order 0.1 which suggests that the solution was generally stable. In Tables 3 and 4, the surface precipitation estimates, R_s, are compared with ground truth, R_T, and the radar data as received from the radar site, R_m. R_s was also estimated using the KBD correction scheme to act as control.

These selected case studies are now discussed individually.

15th Oct 1987

The 15th Oct 1987 provided an ideal opportunity to test the multiple-beam method as inspection of a time series of Chilbolton radar RHI scans showed marked temporal changes in the profile shape, including the period of complete evaporation noted in the previous section. Fortunately, operational radar data were still available for this date. As in the simulation experiment, the Chilbolton radar data were used to provide ground truth. The beam width of the Chilbolton radar is only 0.25 deg., and at 60 km range, the sample volume is $\approx$ 250x300x250 m. Data from all Chilbolton pixels lying within the same 5km operational radar pixel were grouped together and also assigned to height bands 200m deep. The average reflectivity factor within the band centred at 500m above sea level was assumed to give the best estimate of the true equivalent surface precipitation rate. Quality control was applied to ensure that there were sufficient data at this level and to minimize contamination by ground clutter. Data from the operational radar at Clee Hill (located about 160 km north of Chilbolton) were corrected using the multiple-beam scheme. Data were considered to be collocated if the two radars scanned the same pixel within two minutes of each other. Little meteorological data survives for this case so it was necessary to estimate the height of the freezing level and the cloud top height from examination of Chibolton RHI scans. The comparison area was between 150 and 170 km range from Clee Hill. As mentioned above, the Chilbolton RHI scans show complete evaporation before 1100UTC but increasing fraction reaching the ground in the hour following. Between 1200UTC and 1500UTC, the freezing level rose rapidly to about 3 km with the precipitation top at about 6 km. About 1500UTC, the top of the precipitation layer suddenly fell to about 4 km with an associated increase in the reflectivity gradient above the freezing level. In Fig 10, the time series of a_5 from the correction of individual radar images at 5 minute intervals may be compared with hourly average values of a_5 estimated directly from the Chilbolton profiles.

The correction scheme successfully followed the main trends in the profile shape. When the precipitation band first entered the Clee Hill radar area from the south, most pixels showed evidence of evaporation. As the precipitation band progressed further towards the radar, the method produced decreasing values of a_5 as the area of rain within the radar area increased. For comparison, multiple-beam method was also applied to data from the operational radar at Chenies, about 150 km to the south east of Clee Hill. The time series of a_5 from Chenies is also plotted in Fig 10 and shows similar trends to that from Clee Hill, although the highest values of a_5 were close to zero, compared to a maximum of 1.9 km^{-1} from Clee Hill. The area of total evaporation probably constituted a smaller fraction of the total area of precipitation detected by Chenies. Also, the transition from solutions with $a_5 \approx -2$ km^{-1} to $a_5 \approx -6$ km^{-1}, associated with the decrease in the depth of the precipitation layer, occurred about an hour earlier. Nevertheless, the similarities demonstrate the close correspondence between a_5 estimated from the Clee Hill data and that observed near Chilbolton is not fortuitous and the scheme showed some skill in identifying trends in the reflectivity profile shape.

Unfortunately, there is some doubt about the accuracy of the both the Clee Hill and Chilbolton radar calibrations on this day, so quantitative evaluation of the corrected data is confined to the period when most precipitation was evaporating and the uncertainty in the precipitation rates will not have affected the conclusions. The evaporation obviously resulted in $\overline{(R_m - R_T)}$ being an overestmimate of the surface rate. This overestimation was made worse by the assumption of a climatalogical ice profile shape in the KBD method whereas $\overline{(R_s - R_T)}$ for the multiple-beam method was < 0.2 mmh^{-1} for the period 1000 - 1200UTC (Table 3)

13th Nov 1991

Profiles of reflectivity factor in convection commonly show a large gradient in reflectivity factor near to the top of the precipitation layer and relatively smaller gradients close to the freezing level (see e.g. Illingworth *et al*, 1987). This appears to have been the case on the 13th Nov 1991, when widespread showers in a westerly airstream affected Wales. Some coastal observation sites reported hail in some of the showers. Radar data at 5 minute intervals from the operational radar in south west Wales (Dyfed) were corrected and integrated to form hourly totals for comparison with gauge data. Comparison results from gauges at ranges beyond 100 km are summarized in Table 3 and from within 100km of the radar in Table 4. Precipitation was detected on average over only about 15% of the radar area of coverage ($\approx$ 900 pixels). Even so, the range of a_5 was surprisingly small, from -0.3 to 0.4 km^{-1}, which confirms the stability of the solution. Verification of radar estimates of the surface precipitation rate are very difficult in such synoptic conditions because representativeness errors in the radar-gauge comparisons probably make a large contribution to the differences. However, the results in Table 2 suggest that the data as received from the radar site represented a slight overall underestimate of the gauge totals beyond 100 km range. The KBD scheme applied large corrections which turned this underestimate into an overestimate and significantly increased the RMS error. The multiple-beam scheme avoided this and produced much better hourly total estimates at ranges between 100 and 150 km. However, at extreme range, the hourly totals were much lower than some gauge accumulations, although radar detection failures may have contributed to this result more than rate underestimation. Although the multiple-beam method slightly increased the bias error compared to the other corrections, the larger differences were reduced sufficiently to give a much lower RMS error than for the KBD method.

8th Jan 1992

This case (along with the continuation on the 9th Jan, see below) is one of persistent moderate rainfall in a wide band across Wales. On the 8th Jan, a pronounced fall off was observed in rainfall rates measured by the radar beyond the bright band over the Welsh mountains. Hourly integrations of uncorrected radar data were generally much lower than gauge accumulations at long range (Table 3), confirming the need for substantial long range corrections. To reduce the impact of radar detection failures on these differences, comparisons were rejected unless all the radar samples during the hour recorded precipitation in the gauge pixel. Unfortunately, the corrections from the multiple-beam method were too small because the derived values of a_5 were too high (≈ -0.7, see Fig 10) The result was a small increase in the bias error compared to the radar site data, although the overall RMS difference between radar and gauge totals was slightly reduced (Table 2). Possible reasons for the overall underestimation in the required correction are spatial variations in the profile shape across the area of radar coverage, errors in the freezing level height or the orographic growth parametrization. This case is particularly sensitive to the latter because of the low freezing level and the large orographic corrections applied close to the radar. It was interesting that a single image produced a value of $a_5 = -1.9$ km^{-1} (see Fig 10), suggesting the existence of another minimum in the penalty, with much larger implied range corrections. However, J/N for this solution was about twice as large as that for the higher values of a_5.

The bright band parametrization was notably successful in reducing errors closer to the radar (Table 3), with both the KBD and multiple-beam methods largely eliminating the bias error and reducing the RMS error by more than 60% compared to the radar site data (Table 3).

9th Jan 1992

Subjective examination of the Dyfed radar images during the period 0000 - 0900UTC on the 9th Jan 1992 suggested that the fall off in measured rainfall rates with range became smaller with time, particularly after about 0400UTC, and very little range correction appeared necessary over Wales by 0900UTC. For this reason, it was decided to split this case into two periods; before and after 0400UTC. The multiple-beam scheme produced much better long-range corrections in this case than on the 8th Jan. a_5 was mainly < -1.0 km^{-1} up until 0400UTC when there was an abrupt change to higher values which persisted for much of the remainder of the period. The KBD scheme overestimated the corrections beyond 100 km range after 0400UTC with a mean difference between radar and gauge estimates of just over 1 mmh^{-1} (Table 3). A single comparison difference of over 10 mmh^{-1} was eliminated from this analysis as it was unrepresentative of the data as a whole and would have dominated the overall result. The multiple-beam scheme reduced the mean error to less than 0.2 mmh^{-1} but at the price of a small increase in the RMS difference.

The bright band errors were considerably reduced up until about 0400UTC but thereafter, the bright band became very intense and large bias errors of over 2 mmh^{-1} (equal to about half the average gauge rate) persisted even after corrections had been applied. Nevertheless, the RMS differences at ranges < 100 km from the multiple-beam method were about one third of those for the radar site data.

The figures for the absolute mean differences and RMS differences from the cases 13th Nov 1991, 8th and 9th Jan 1992 were averaged together. At the longer ranges, the new method reduced the mean differences by 27% compared to data from the radar site but with only a marginal decrease in RMS error. This compares to the KBD method which only reduced the mean difference by 6% and increased the RMS difference. There is, of course, considerable

uncertainty in statistics based on a small number of cases. Whilst representativeness errors undoubtably contribute significantly to the radar-gauge differences, it is recognised that the modest reduction in radar gauge differences resulting from the multiple-beam method suggests that the level of improvement in long range correction achieved in the simulation experiments is unlikely to be matched in reality. It is interesting that almost all values of J/N from the 4 cases were in the range 0.05 - 0.2; up to a few times larger than in the simulation experiments. This suggests that the spatial variability in profile shape incoporated in the simulation method underestimated the true level. The penalty may also have been increased by measurement uncertainties (e.g. in the radar horizon and beam elevations).

In view of the similarities between the bright band and orographic growth parametrizations in the multiple-beam and KBD methods, it is surprising the the multiple-beam methods gave improved results at ranges less than 100 km (a 65% reduction in the average RMS difference compared to 57% for KBD). The improvement may be attributed to differences in the assumptions involved in the two methods, particularly when the bright band is very low and intersects the orographic growth layer.

Having applied the multiple-beam method to selected cases, it was then applied to 7 cases of mainly widespread, wintertime frontal rainfall selected at random and used previously in the evaluation of the KBD correction method. Subjective examination of radar images from these cases suggested that the reflectivity factor profiles were closer to the climatalogical average compared to the selected cases, and therefore the scope for improved long range corrections was also much lower. Data from the Wardon Hill radar were corrected as KBD found this radar to be accurately calibrated during the relevant period. There was evidence that this radar has a lower effective MDS than the other radars in the UK network (Kitchen and Brown, 1992). Accordingly, it was decided to use a value of $\epsilon = 0.1$ in equation 6 applied to data from this radar.

Time series of the values of a_5 in these cases are shown in fig 11. The values were mainly ≈ -2 km^{-1}; close to the climatalogical average (see Fig 3). The exceptions were in the case of the snow showers on the 7th Feb 1991, when $a_5 \approx -3$ km^{-1} and on the the 8th Mar 1991 when $a_5 \leq -1$ km^{-1} for most of the period. Hourly gauge comparisons provided evidence of the performance of the corrections at long ranges, as almost all Meteorological Office gauges within the area of Wardon Hill radar coverage are at ranges > 125 km. The small amount of gauge data available necessitated the relaxation of the detection criterion to a requirement that the radar detected precipitation in the gauge pixel in more than half the samples during the hour. Even so, there were no valid comparisons for the 7th Feb 1991 case and for the 27th Feb 1991, gauge data were obtained from the network in the London area maintained by the Thames area of the National Rivers Authority. The results in Table 5 do not show the multiple-beam method producing a consistent improvement over the KBD method at long range, or indeed over the fixed range corrections applied at the radar site. For example, the gauge comparisons for the 8th Mar 1991 suggest that the high values of a_5 resulted in detrimental corrections. Nevertheless, the average RMS difference over the 6 cases in Table 5 for both KBD and multiple-beam methods were marginally smaller than for the radar site data (reductions of 12 and 13% respectively). The multiple-beam method achieved a more worthwhile reduction of 30% in the overall absolute mean difference.

For verification at shorter ranges, Chilbolton RHI data were again used to derive estimates of the surface precipitation rate within Wardon Hill pixels within 60 km range of Chilbolton.. The comparison pixels were at ranges between 40 and 125km from Wardon Hill, i.e. at moderate ranges where the corrections were dominated by the bright band. Comparisons were rejected from a range of azimuths from Wardon Hill within which the lowest elevation Wardon Hill radar beam suffers from serious occultation. Data were considered to be collocated if both radars

sampled the same pixel within two minutes of each other. The results of these comparisons are shown in Table 6. The multiple-beam method gave almost identical results to the KBD scheme, which is to be expected in cases where the bright band is at moderate range. This is confirmation that the large scale of the mimimization problem did not prove to be an obstacle to reaching solutions of acceptable accuracy. The corrections reduced the mean difference in 6 cases compared to the data as received from the radar site, with no increase in the magnitude of the difference in the other case. Similarly, the RMS difference was substantially reduced in 4 cases and only marginally increased in one. Both correction methods reduced the RMS difference computed over all 7 cases by 53%. The effectiveness of the corrections was almost entirely due to the success of the bright band parametrization; orographic corrections were generally small.

5. CONCLUSIONS

To meet a requirement for quantitative estimates of surface precipitation rate over the UK in wintertime, an attempt must be made to correct radar data from ranges where the lowest elevation beam is mainly above the freezing level. A method of radar data correction has been devised in which radar data from several beam elevations are used in an attempt to improve long range corrections. Similar to other methods, an assumption of horizontal homogeneity in the reflectivity factor profile shape above the freezing level was required. Unlike other methods, the profile below the freezing level is constrained by simple pixel-scale parametrizations of the bright band and orographic growth. The difference between the idealized profile and the radar observations is expressed as a penalty function which is minimised by iteration. The form of the idealized profile and the function fitted to the beam power profile were chosen so that the penalty and its gradients could be expressed as analytic functions. Despite the large scale of the problem, with up to a few thousand variables, there were no problems in arriving at a satisfactory solution. The method gives some weight to zero signals from radar beams above the lowest in elevation and the precise solution is sensitive to the weighting and also the MDS for the particular radar.

The enormous difficulties of correcting radar data obtained from above the freezing level were recognised. A short study of real reflectivity factor profiles suggested that the new approach could improve long range corrections in some cases, but the spatial and temporal variability in the profile would invalidate the assumptions at other times. A simulation experiment demonstrated that the method had considerable potential to reduce long-range bias errors when conditions were favourable. The mean absolute bias at 200km range over 12 cases of widespread rain was reduced by 64% over the raw radar data and about 35% over corrections based upon the use of a climatalogical reflectivity factor profile shape. However, the inability to resolve some significant variability in the reflectivity factor profile shape resulted in detrimental corrections in some cases. The final penalty was found to be correlated with the the error in the surface precipitation rate estimates.

Tests on operational radar data generally support the conclusions from the simulation experiment, although the demonstrable quantitative improvement was much smaller. In a case of evaporation, where the reflectivity factor increased with height above the freezing level, the use of the higher elevation beam data in the multiple-beam method succesfully avoided the spurious corrections resulting from an assumption of a climatalogical profile shape. As in the simulation experiment, the new method failed to show consistent benefit compared to simpler methods in typical wintertime precipitation. However, there were overall reductions in both bias and random errors at long range.

Future development should be focussed on increasing the spatial variability in the profiles which can be resolved. This implies either the use of smaller correction domains or enabling the

variables which describe the profile to vary smoothly in space in some way. The simplest way of reducing the domain size would be to divide the radar area up into two or more sectors and process the data from each independently. A more sophisticated approach could be to apply the method to all the data initially, and then examine the contribution to the penalty J from each pixel. If some pixels were found to be contributing disproportionately to the penalty, this could be indicatative of systematic differences in the reflectivity factor profile. These pixels could then be placed in a separate correction domain and the method reapplied to the two regions. It could be imagined that this sort of approach would be advantageous where, for example, deep convection was embedded within more widespread frontal rainfall. The magnitude of J in individual pixels may also be of use in quality control. For example, radar measurements at different elevation angles during anaprop conditions should be inconsitent with the idealized reflectivity factor profile and produce anomalously high values of J. Eyre *et al* (1993) describes a similar application relating to quality control of satellite temperature soundings.

The value of the penalty could be given further quantitative significance by using a more standard formulation of the penalty function, in which the penalty is normalized by the error variance.

$$J = \sum \frac{X^2}{\sigma_X^2} \tag{12}$$

where, in this case,

$$X = \sum_i \sum_n \log \frac{Z_c}{Z_m} \tag{13}$$

As before, Z_c is the reflectivity factor calculated from the idealized profile; Z_m is the measurement; the sums are over i wet pixels in the radar image and n radar beams. The error variances σ_X^2 include contributions from errors in the radar measurements, the reflectivity profile specification and in the various parametrizations; all of which have to be estimated. This penalty formulation has not yet been adopted because, despite attempts to tune the error variances, it has so far failed to deliver improved results in the simulation experiment compared to the empirical version.

In cases of small scale convection, there may be few wet pixels and insufficient information to derive stable, representative values of $a_{j'}$. It is therefore suggested that in some circumstances, it may be best to revert to the simpler KBD method.

ACKNOWLEDGEMENTS

The idea of using a penalty minimization method to estimate surface precipitation rates from radar data from several elevation angles was suggested by both C Beneti (Reading Univ.) and Dr B Macpherson (Meteorological Office) independently. Dr B Macpherson also gave advice on the solution method. R Brown of the Meteorological Office provided general advice and direction to the work. The Chilbolton radar data were supplied by the Radio Communications Research Unit of the Rutherford Appleton Laboratory. John Goddard and Kevin Morgan of the Unit gave advice on its processing. Some of the hourly gauge data were provided by the Thames region of the National Rivers Authority.

APPENDIX

The algebra involved in producing formulae for the value of the penalty and its gradients is long but straightforward. Only some of the key expressions are written down here.

To compute Z_c from equation 11, an expression is required for $\int_\alpha^\beta Z(\phi)\,P(\phi)\,d\phi$. For layers in the idealized reflectivity factor profile below the freezing level, the reflectivity factor is assumed to change linearly with height (Fig 1) and for small values of $(\gamma+\phi)$, the reflectivity factor will also be approximately linear in ϕ. Between levels j and $j+1$, we can write:

$$Z(\phi) = Z_j + (Z_{j+1} - Z_j)\frac{(\phi - \phi_j)}{(\phi_{j+1} - \phi_j)}$$

Then

$$\int Z(\phi)\,P(\phi)\,d\phi = \left(Z_j - \frac{(Z_{j+1} - Z_j)\phi_j}{(\phi_{j+1} - \phi_j)}\right)\int P(\phi)\,d\phi + \frac{(Z_{j+1} - Z_j)}{(\phi_{j+1} - \phi_j)}\int \phi\,P(\phi)\,d\phi \qquad (14)$$

The integral in the first term is simple. For the second term on the RHS;

$$\int \phi\,P(\phi)\,d\phi = \frac{1}{2}\int \phi\,\cos(k\phi) + \frac{1}{2}\int \phi\,d\phi$$

$$= \left[\frac{\phi^2}{4} + \frac{1}{2k^2}(\cos(k\phi) + k\phi\sin(k\phi))\right]_\alpha^\beta \qquad (15)$$

For profile layers 5 and 6,

$$\int Z(\phi)\,P(\phi)\,d\phi = Z_j\int e^{a_{j'r}(\phi-\phi_j)}\,P(\phi)\,d\phi$$

$$= \frac{Z_j\,e^{-a_{j'r}\phi_j}}{2}\int e^{a_{j'r}\phi}\cos(k\phi)\,d\phi + \frac{Z_j\,e^{-a_{j'r}\phi_j}}{2}\int e^{a_{j'r}\phi}\,d\phi \qquad (16)$$

$\int e^{C\phi}\,cos(c\phi)$,where c and C are constants, is a standard integral with the solution

$$\frac{e^{C\phi}}{C^2+c^2}(C\cos(c\phi) + c\sin(c\phi))$$

Therefore,

$$Z_j\int e^{a_{j'r}(\phi-\phi_j)}\,P(\phi)\,d\phi = \frac{Z_j\,e^{-a_{j'r}\phi_j}}{2}\left[\frac{e^{a_{j'r}\phi}}{(a_{j'r})^2+k^2}(a_{j'r}\cos(k\phi) + k\sin(k\phi))\right]_\alpha^\beta + \frac{Z_j\,e^{-a_{j'r}\phi_j}}{2a_{j'r}}\left[e^{a_{j'r}\phi}\right]_\alpha^\beta \qquad (17)$$

The calculation of $\partial Z_c/\partial Z_b$ involves differentiation of the terms in equations 14 and 16. This is straightforward, only requiring additional expressions for $\partial Z_S/\partial Z_b$ (for layer 1) and $\partial(Z_B - Z_b)/\partial Z_b$ (for layers 3 and 4) .

From equation 2,

$$\frac{\partial Z_S}{\partial Z_b} = \mu A\left(\left(\frac{Z_b}{A}\right)^{1/\mu} + O\right)^{(\mu-1)}\left(\frac{(1/\mu)\,Z_b^{\left(\frac{1-\mu}{\mu}\right)}}{A^{1/\mu}}\right) \qquad (18)$$

and from equation 4

$$\frac{\partial(Z_B - Z_b)}{\partial Z_b} = \frac{357.8\, Z_b^{0.42}}{\Delta h_B} \tag{19}$$

$\partial Z_c/\partial a_{j'}$ contains contributions from layers 5 and 6 only. Differentiating the LHS of equation 17,

$$\begin{aligned}\frac{\partial}{\partial a_{j'}}\left(Z_j \int e^{a_{j'} r(\phi-\phi_j)}\, P(\phi)\, d\phi\right) &= \frac{\partial Z_j}{\partial a_{j'}} \int e^{a_{j'} r(\phi-\phi_j)}\, P(\phi)\, d\phi + \\ & Z_j \frac{\partial}{\partial a_{j'}}\left(\int e^{a_{j'} r(\phi-\phi_j)}\, P(\phi)\, d\phi\right)\end{aligned} \tag{20}$$

An expression for the second term on the RHS of equation 20 is provided by differentiation of the terms on the RHS of equation 17.

$$\begin{aligned}Z_j \frac{\partial}{\partial a_{j'}}\left(\int e^{a_{j'} r(\phi-\phi_j)}\, P(\phi)\, d\phi\right) &= \frac{Z_j}{2}\Bigg[e^{a_{j'} r(\phi-\phi_j)}\left(\frac{r}{(a_{j'}r)^2 + k^2}\right)\cos(k\phi) + \\ & e^{a_{j'} r(\phi-\phi_j)}\left(\frac{-2a_{j'}r^2}{((a_{j'}r)^2 + k^2)^2}\right)(a_{j'}r\cos(k\phi) + k\sin(k\phi)) + \\ & r(\phi-\phi_j)e^{a_{j'} r(\phi-\phi_j)}\left(\frac{1}{(a_{j'}r)^2 + k^2}\right)(a_{j'}r\cos(k\phi) + k\sin(k\phi)) + \\ & e^{a_{j'} r(\phi-\phi_j)}\left(\frac{-1}{a_{j'}^2 r}\right) + \frac{r(\phi-\phi_j)}{a_{j'}r}e^{a_{j'} r(\phi-\phi_j)}\Bigg]_\alpha^\beta\end{aligned} \tag{21}$$

The first term on the RHS of equation 20 is zero for layers 5 and 6 considered separately, but there is a contribution to $\frac{\partial Z_c}{\partial a_5}$ from $\frac{\partial Z_6}{\partial a_5}$, as the reflectivity factor at level 6 is defined by:-

$$Z_6 = Z_5 e^{a_5 r(\phi_6 - \phi_5)}$$

REFERENCES

Andrieu, H. and Creutin, J. D. 1995 Identification of vertical profiles of radar reflectivity for hydrological applications using an inverse method. Part I: Formulation. *Journal of Appl. Met.*, **34**, 225-259.

Carpenter, K. M. 1983 Calculating vertical reflectivity profile (sic.) Meteorological Office, Radar Research Laboratory, Forecasting Research Group, Report No 47.

Davies, A. G. 1992 Bright band correlations for layer precipitation; the comparison of Chilbolton radar data and Hardaker model output. Meteorological Office (Forecasting Research Division) Tech. Report No 32.

Eyre, J. R., Kelly, G. A., McNally, A. P., Anderson, E. and Persson, A. 1993 Assimilation of TOVS radiance information through one dimensional multiple-beam analysis *Quart. J. Roy. Meteor. Soc.*, **119**, 1427-1463.

Fabry, F., Austin, G. L., and Tees D. 1992 The accuracy of rainfall estimates by radar as a function of range. *Quart. J. Roy. Meteor. Soc.*, **118**, 435-453.

Gray, W. 1991 Vertical profile corrections based on EOF analysis of operational data. Preprints, 25th Int. Conf. on Radar Meteorology, Paris, 1991, American Met. Soc., 821-823.

Harris, F. I. 1977 The effects of evaporation at the base of ice precipitation layers: Theory and radar observations. *Journal of Atmos. Science*, **34**, 651-672

Harrold, T. W. and Kitchingman, P. G. 1975 Measurement of surface rainfall using radar when the beam intersects the melting layer. American Met. Soc., Proc. 16th Radar Met. Conf., Houston, Tex., 1975, 473-478.

Hill, F. F. 1983 The use of annual average rainfall to derive estimates of orographic enhancement over England and Wales for different wind directions. *J. Clim.*, **3**, 113-129.

Illingworth, A. J., Goddard, J. W. F., and Cherry, S. M. 1987 Polarisation radar studies of precipitation development in convective storms. *Q. J. R. Meteorol. Soc.*, **113**, 445-468.

Kitchen, M. and Brown, P. M. 1992 Detection of precipitation by radars in the UK weather radar network. Meteorological Office, Short Range Forecasting Division, Technical Report No 12.

Kitchen, M., Brown, R. and Davies, A. G. 1994 Real-time correction of weather radar data for the effects of bright band, range and orographic growth in widespread rain. *Q. J. R. Meteorol. Soc.*, **120**, 1231-1254.

Kitchen, M. and Jackson, P. M. 1993 Weather radar performance and long range - Simulated and observed. *Journal of Appl. Met.*, **32**, 975-985.

Koistinen, J. 1991 Operational correction of radar rainfall errors due to the vertical reflectivity profile. American Met. Soc., Preprints, 25th Int. Conf. on Radar Meteorology, Paris, 1991, 91-94.

Smith, C. J. 1986 The reduction of errors caused by bright bands in quantitative rainfall measurements using radar. *J. Atmos. Ocean. Technology*, **3** 129-14

TABLE 1. RESULTS FROM THE SIMULATION EXPERIMENT

Date	Hour (UTC)	a_5 km^{-1}	75km range Meas (mmh^{-1})	75km range Cont (mmh^{-1})	75km range M-B (mmh^{-1})	200km range Meas (mmh^{-1})	200km range Cont (mmh^{-1})	200km range M-B (mmh^{-1})
14Oct87	17-18	-4.4	0.50	0.57	-0.48	-1.49	-1.07	-0.87
15Oct87	10-11	2.2	0.02	0.02	0.04	0.47	2.85	0.07
15Oct87	11-12	0.4	0.12	0.04	0.08	0.07	1.25	0.12
19Nov87	15-16	-0.2	0.20	0.20	0.24	-0.40	1.13	-0.09
05Jan88	04-05	-1.3	3.03	0.02	-0.09	-2.18	0.28	-0.04
12Jan88	23-24	-3.4	0.96	0.09	0.07	-0.98	-0.58	0.13
13Jan88	00-01	-2.4	1.74	0.05	-0.08	-1.92	-1.27	-0.92
13Jan88	02-03	-0.5	1.25	0.15	0.09	-0.87	1.33	-0.09
09Feb88	02-03	-0.8	0.58	0.15	0.08	-1.34	0.48	-0.32
23Sep88	02-03	-1.6	0.67	0.17	0.19	-0.53	1.53	1.97
28Sep88	15-16	-0.8	0.49	-0.41	-0.36	-1.72	0.61	-0.11
14Mar89	17-18	-1.0	1.97	-0.64	-0.65	-2.59	0.15	-0.52
10Apr89	14-15	-0.4	-0.05	-0.27	0.28	-1.10	0.38	-0.25
11Apr89	10-11	-1.4	1.20	0.17	0.02	-2.40	-0.83	-0.84
12Apr89	09-10	-1.8	0.26	-0.03	-0.03	-0.80	0.80	0.80

a) The values under Meas are $\overline{R_m - R_T}$; those under Cont are $\overline{R_s - R_T}$ from the control method, and under M-B are $\overline{R_s - R_T}$ from the multiple-beam correction method.
b) The first three cases show evidence of complete evaporation within a layer above the freezing level.
c) The statistics in the last three columns are for 200km range except where the simulation indicated that the radar would be unable to detect precipitation at this range, when the results for 175km range were substituted. d) The values of a_5 refer only to the multiple-beam method.

TABLE 2. VERIFICATION CASE STUDIES

Date		freezing level (km)	synoptic conditions
15Oct91	Clee	1.5-3.0	evaporation ahead of warm front
13Nov91	Dyfed	0.8	scattered showers
08Jan92	Dyfed	1.5	warm front
09Jan92	Dyfed	1.5-0.5	occlusion
07Feb91	Wardon	< 0	snow showers
21Feb91	Wardon	1.6	warm sector
22Feb91	Wardon	1.3	warm front/sector
27Feb91	Wardon	1.1	weak fronts
08Mar91	Wardon	2.1	warm front/sector
16Mar91	Wardon	2.2	cold front
18Mar91	Wardon	2.6	warm front

TABLE 3. VERIFICATION IN SELECTED CASES AT RANGES > 100 km.

Date	Time (UTC)	No	$\overline{R_T}$ (mmh^{-1})	$\overline{R_s - R_T}$ Site (mmh^{-1})	$\overline{R_s - R_T}$ KBD (mmh^{-1})	$\overline{R_s - R_T}$ M-B (mmh^{-1})	RMS $R_s - R_T$ Site (mmh^{-1})	RMS $R_s - R_T$ KBD (mmh^{-1})	RMS $R_s - R_T$ M-B (mmh^{-1})
15Oct87	10-1100	56	0.01	-0.52	-2.88	-0.09	0.54	3.00	0.11
15Oct87	11-1200	81	0.20	-0.39	-3.12	-0.16	0.48	3.45	0.28
13Nov91	00-1200	53	0.64	-0.25	0.21	-0.33	0.67	0.97	0.65
08Jan92	18-2400	37	2.28	-1.22	1.06	-1.26	1.94	1.76	1.88
09Jan92	00-0400	15	2.31	-0.81	-0.33	-0.29	1.17	0.81	1.11
09Jan92	04-0900	20	3.89	-0.56	1.08	-0.19	2.79	3.89	2.81

a) No is the number of individual comparisons.
b) Three alternative estimates of R_s were compared; the data as received from the radar site (Site), from the KBD scheme, and using the new multiple-beam method (M-B). Other symbols are defined in the text.
c) The verification in the 15th Oct 1987 case was against instantaneous near-surface rates derived from the Chilbolton radar. In all other cases (used also in Table 4), the comparison was between hourly gauge accumulations and integrations of 5 minute radar data.

TABLE 4. VERIFICATION IN SELECTED CASES AT RANGES < 100 km.

Date	Time (UTC)	No	$\overline{R_T}$ (mmh^{-1})	$\overline{R_s - R_T}$ Site (mmh^{-1})	KBD (mmh^{-1})	M-B (mmh^{-1})	RMS $R_s - R_T$ Site (mmh^{-1})	KBD (mmh^{-1})	M-B (mmh^{-1})
13Nov91	00-1200	34	0.53	0.02	0.15	-0.11	0.42	0.52	0.41
08Jan92	18-2400	27	1.11	0.83	0.06	-0.05	1.43	0.55	0.55
09Jan92	00-0400	20	1.30	1.56	0.43	0.26	2.55	0.83	0.65
09Jan92	04-0900	23	2.47	4.20	2.62	2.02	9.03	3.79	3.08

TABLE 5. VERIFICATION IN TYPICAL CASES, MAINLY AT LONG RANGE

Date	Time (UTC)	No	$\overline{R_T}$ (mmh^{-1})	$\overline{R_s - R_T}$ Site (mmh^{-1})	KBD (mmh^{-1})	M-B (mmh^{-1})	RMS $R_s - R_T$ Site (mmh^{-1})	KBD (mmh^{-1})	M-B (mmh^{-1})
21Feb91	15-1800	11	1.42	-1.01	-0.89	-0.51	1.19	1.09	0.91
22Feb91	14-2000	28	1.38	-0.62	-0.50	-0.33	1.00	0.90	0.90
27Feb91	16-1900	24	1.56	-1.17	-0.86	0.13	1.51	1.29	1.27
08Mar91	00-0500	36	1.28	-0.10	-0.35	-0.53	0.84	0.86	0.87
16Mar91	11-1530	23	1.29	-0.21	-0.49	0.52	1.07	0.73	0.77
18Mar91	12-2300	55	1.33	-0.60	-0.68	-0.60	1.16	1.24	1.16

Hourly integrations of radar data were comapared with hourly gauge accumulations in all these cases.

TABLE 6 VERIFICATION IN TYPICAL CASES AT MODERATE RANGE

Date	Time (UTC)	No	$\overline{R_T}$ (mmh^{-1})	$\overline{R_s - R_T}$ Site (mmh^{-1})	$\overline{R_s - R_T}$ KBD (mmh^{-1})	$\overline{R_s - R_T}$ M-B (mmh^{-1})	RMS $R_s - R_T$ Site (mmh^{-1})	RMS $R_s - R_T$ KBD (mmh^{-1})	RMS $R_s - R_T$ M-B (mmh^{-1})
07Feb91	03-0800	15	0.27	-0.17	-0.12	0.06	0.28	0.25	0.25
21Feb91	15-1800	63	0.70	0.47	0.09	0.07	0.85	0.32	0.31
22Feb91	14-2000	136	0.94	0.18	-0.10	-0.06	0.92	0.47	0.47
27Feb91	16-1900	43	0.56	0.10	-0.10	-0.10	0.29	0.20	0.20
08Mar91	00-0500	95	0.57	-0.17	-0.02	-0.02	0.54	0.28	0.25
16Mar91	11-1530	84	1.04	0.48	0.00	0.07	1.49	0.60	0.63
18Mar91	12-2300	148	0.46	-0.07	-0.07	-0.04	0.24	0.23	0.25

Verification was against instantaneous near-surface precipitation rates derived from Chilbolton radar data.

Fig 1. The idealized reflectivity factor profile used in the multiple-beam correction method. The various symbols are explained in the text.

Fig 2. A schematic diagram showing how estimates of a_5 were derived from measured reflectivity factor profiles. The crosses are the average measured reflectivity factor in 200m deep layers from RHI scans . Point 'P' is defined by the estimated freezing level height and the value of the background reflectivity factor (see text).

Fig 3. The slope of the reflectivity profile (in dB km^{-1}) in the 2km above the freezing level derived from all Chilbolton profiles during the period Jan - Mar 1988. Only profiles when the freezing level was in the height range 1.0 - 2.5 km were processed. A positive slope indicates the usual decrease in reflectivity factor with height. The equivalent values of a_5 are shown down the right hand side.

Fig 4. The two-way radar beam power profile for an operational radar antenna as measured by the manufacturers and as fitted by a simple cosine function. The one-way half-power beam width is ≈ 0.009 rad. A Gaussian fit to the data (half-width = 0.0057 rad) is also shown for comparison.

Fig 5. Hourly mean reflectivity factor profiles for the initial 12 cases used in the simulation experiment. The values of the reflectivity facator in mm^6m^{-3} from each profile were averaged together but converted to dBZ for plotting.

Fig 6. Bias errors as a function of radar range from the simulation experiment. $(R_s - R_T)$ from the multiple-beam method is shown by the closed circles and from the control method by the open circles. $(R_m - R_T)$ (which is also the error in the first guess) is shown by the crosses and solid line for comparison.

Fig 7. The RMS error in surface estimates of log rainfall rate as a function of the penalty per pixel for the 12 simulation cases shown in Fig 6.

Fig 8. Hourly mean reflectivity factor profiles for three additional cases where there was evidence of the evaporation of ice.

Fig 9. Similar to Fig 6 but for the three evaporation cases of Fig 8.

Fig 10. Time series of a_5 produced by the correction scheme applied to operational radar data from the four selected case studies (solid lines). In the 15th Oct 1987 case, the solid line is from analysis of Clee Hill radar data whereas the dashed line is for the Chenies radar. The circled crosses are average values of a_5 estimated directly from the hourly average Chilbolton reflectivity profiles.

Fig 11. Similar to Fig 10 for analysis of data from the Wardon Hill radar in a further 7 randomly selected cases.

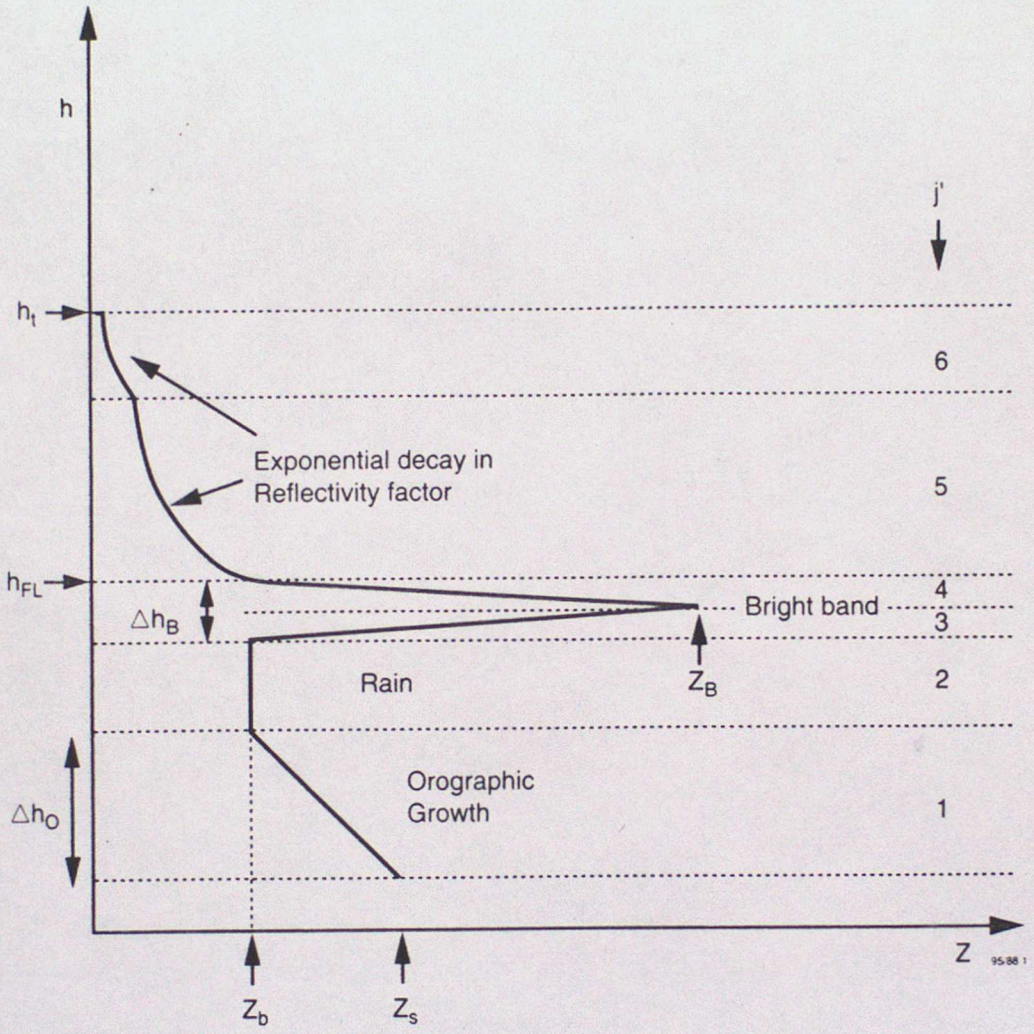

Fig 1. The idealized reflectivity factor profile used in the multiple-beam correction method. The various symbols are explained in the text.

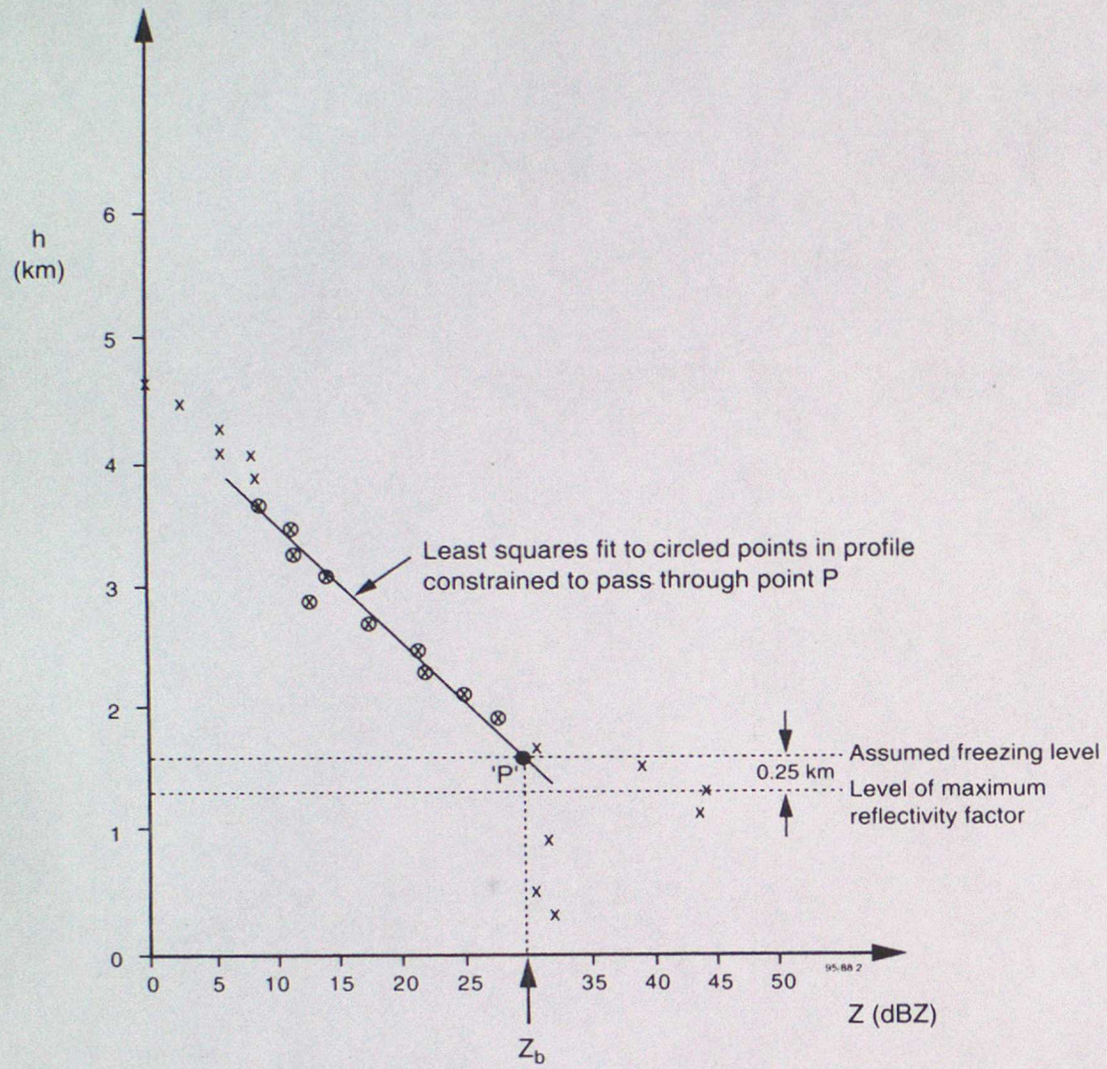

Fig 2. A schematic diagram showing how estimates of a_5 were derived from measured reflectivity factor profiles. The crosses are the average measured reflectivity factor in 200m deep layers from RHI scans . Point 'P' is defined by the estimated freezing level height and the value of the background reflectivity factor (see text).

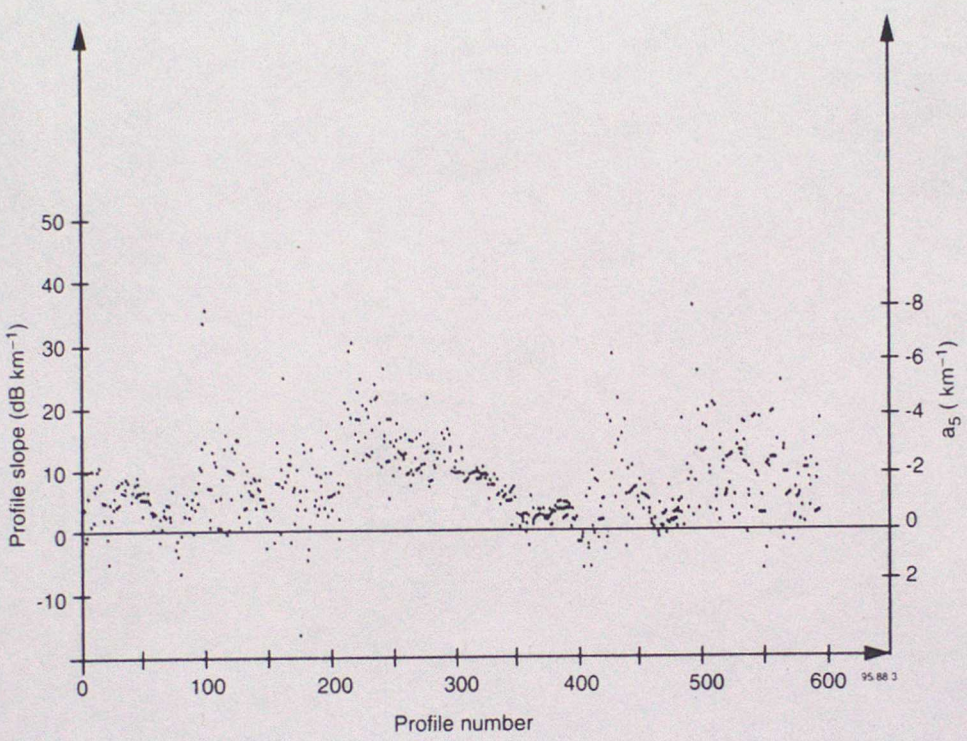

Fig 3. The slope of the reflectivity profile (in dB km^{-1}) in the 2km above the freezing level derived from all Chilbolton profiles during the period Jan - Mar 1988. Only profiles when the freezing level was in the height range 1.0 - 2.5 km were processed. A positive slope indicates the usual decrease in reflectivity factor with height. The equivalent values of a_5 are shown down the right hand side.

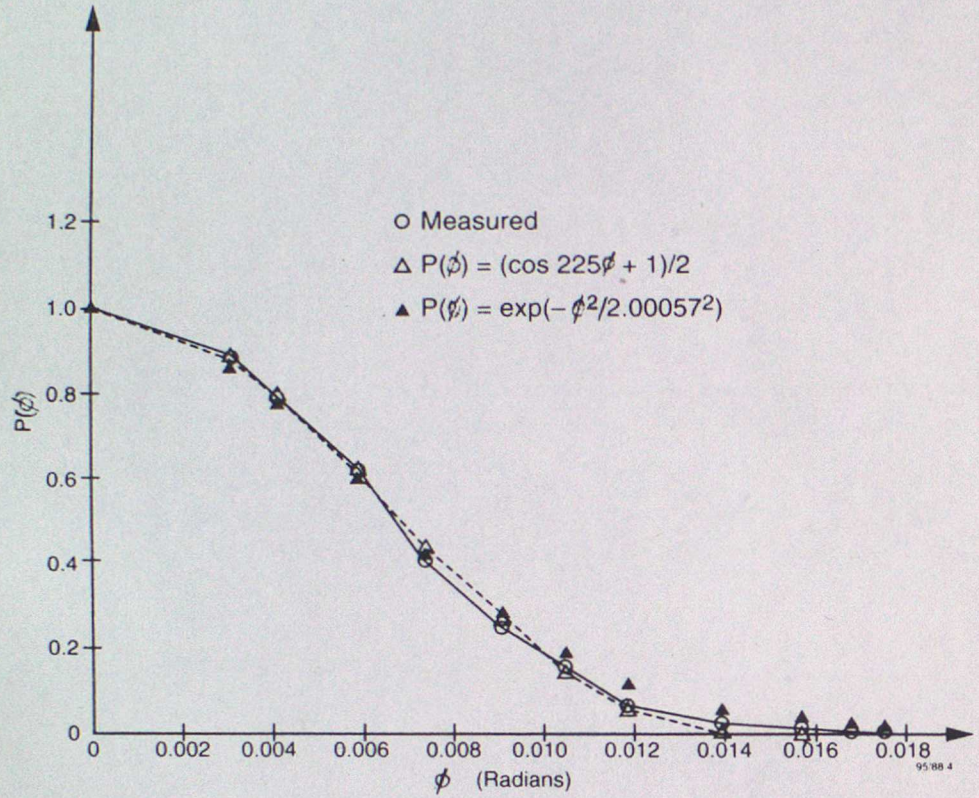

Fig 4. The two-way radar beam power profile for an operational radar antenna as measured by the manufacturers and as fitted by a simple cosine function. The one-way half-power beam width is ≈ 0.009 rad. A Gaussian fit to the data (half-width = 0.0057 rad) is also shown for comparison.

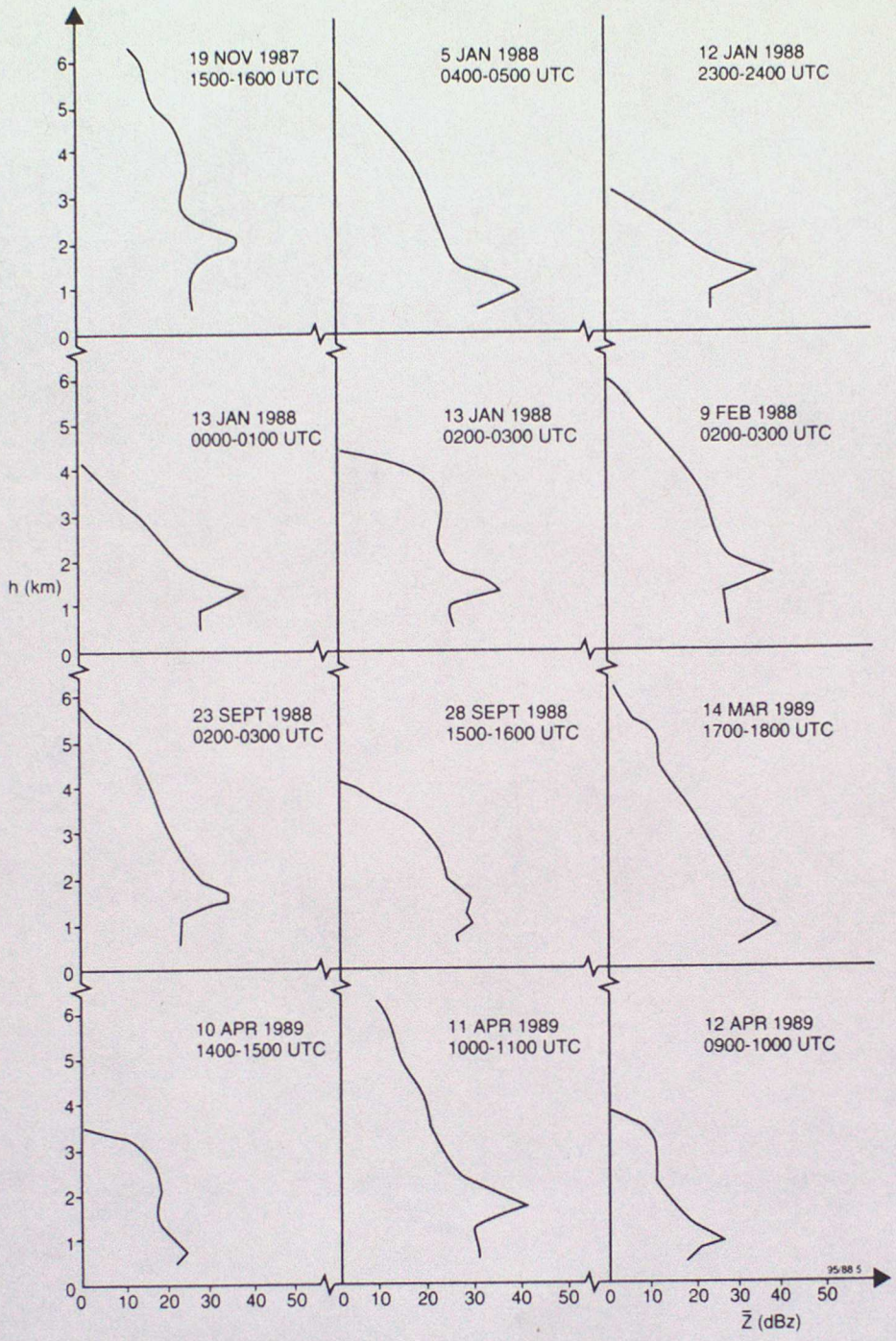

Fig 5. Hourly mean reflectivity factor profiles for the initial 12 cases used in the simulation experiment. The values of the reflectivity facator in mm^6m^{-3} from each profile were averaged together but converted to dBZ for plotting.

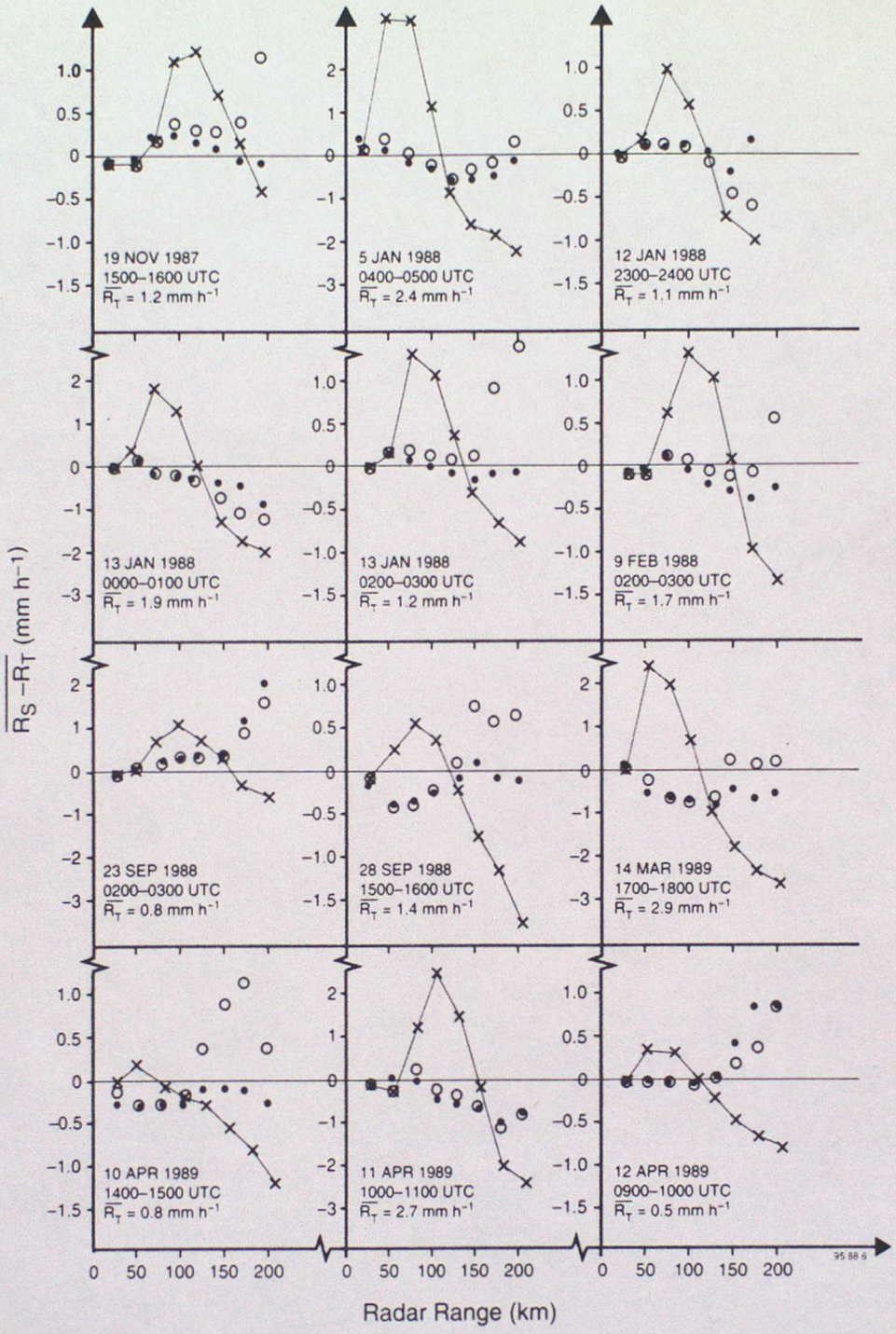

Fig 6. Bias errors as a function of radar range from the simulation experiment. $(R_s - R_T)$ from the multiple-beam method is shown by the closed circles and from the control method by the open circles. $(R_m - R_T)$ (which is also the error in the first guess) is shown by the crosses and solid line for comparison.

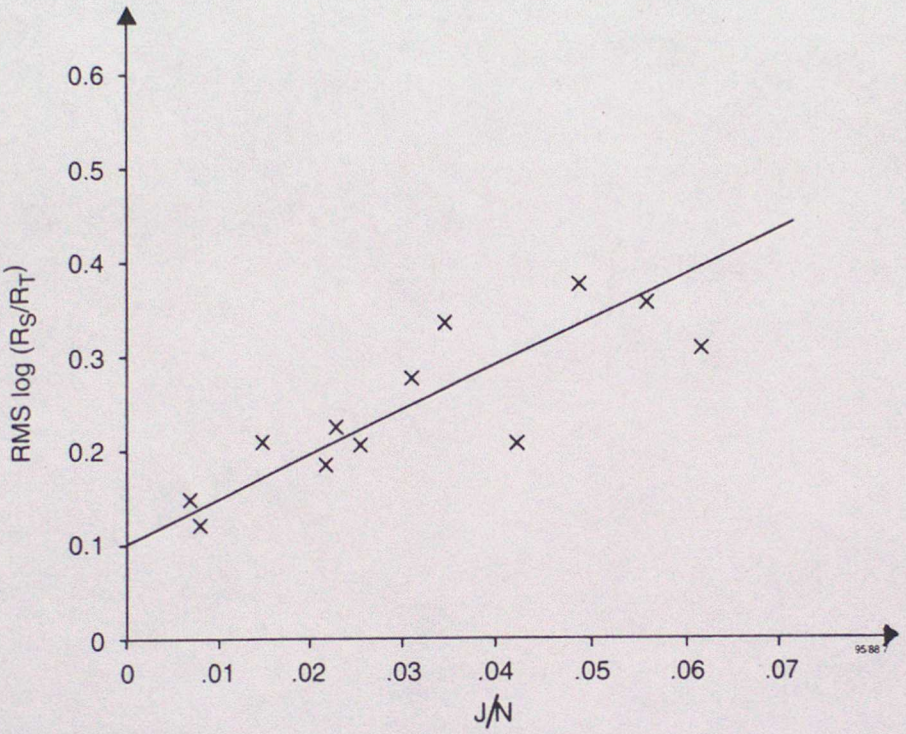

Fig 7. The RMS error in surface estimates of log rainfall rate as a function of the penalty per pixel for the 12 simulation cases shown in Fig 6.

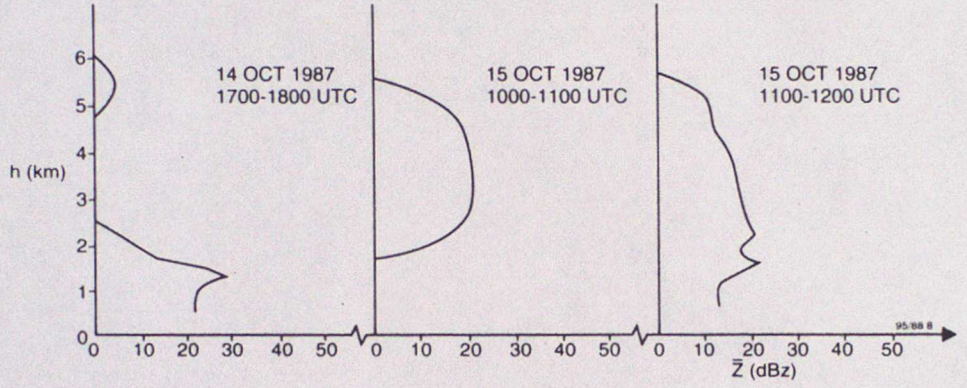

Fig 8. Hourly mean reflectivity factor profiles for three additional cases where there was evidence of the evaporation of ice.

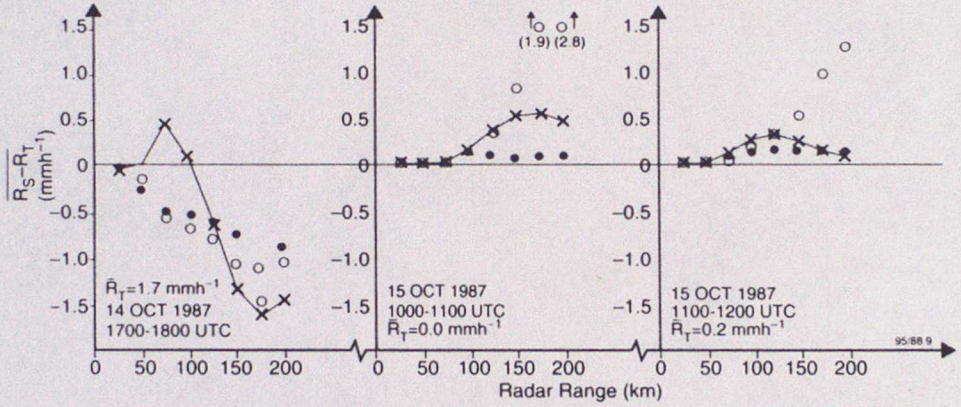

Fig 9. Similar to Fig 6 but for the three evaporation cases of Fig 8.

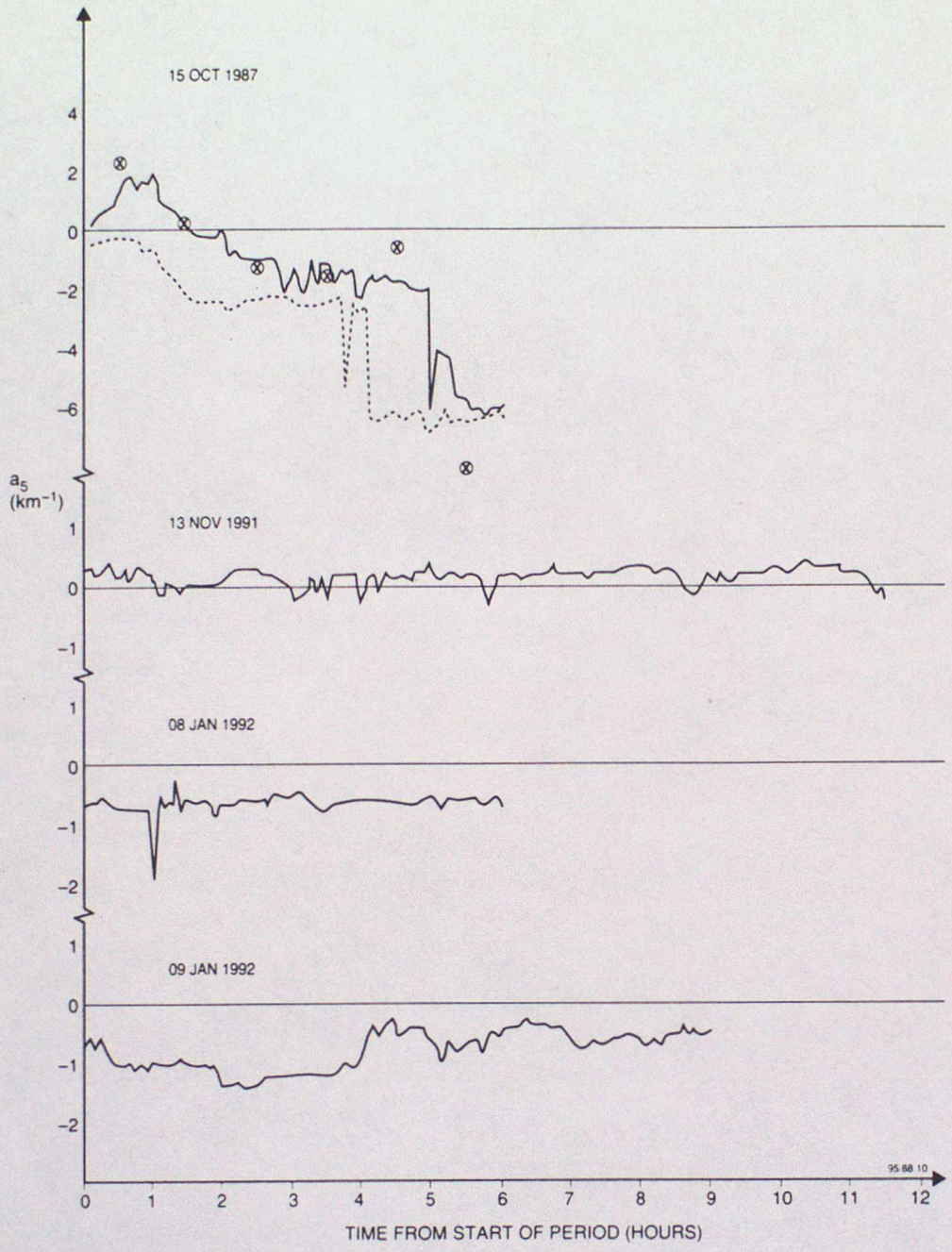

Fig 10. Time series of a_5 produced by the correction scheme applied to operational radar data from the four selected case studies (solid lines). In the 15th Oct 1987 case, the solid line is from analysis of Clee Hill radar data whereas the dashed line is for the Chenies radar. The circled crosses are average values of a_5 estimated directly from the hourly average Chilbolton reflectivity profiles.

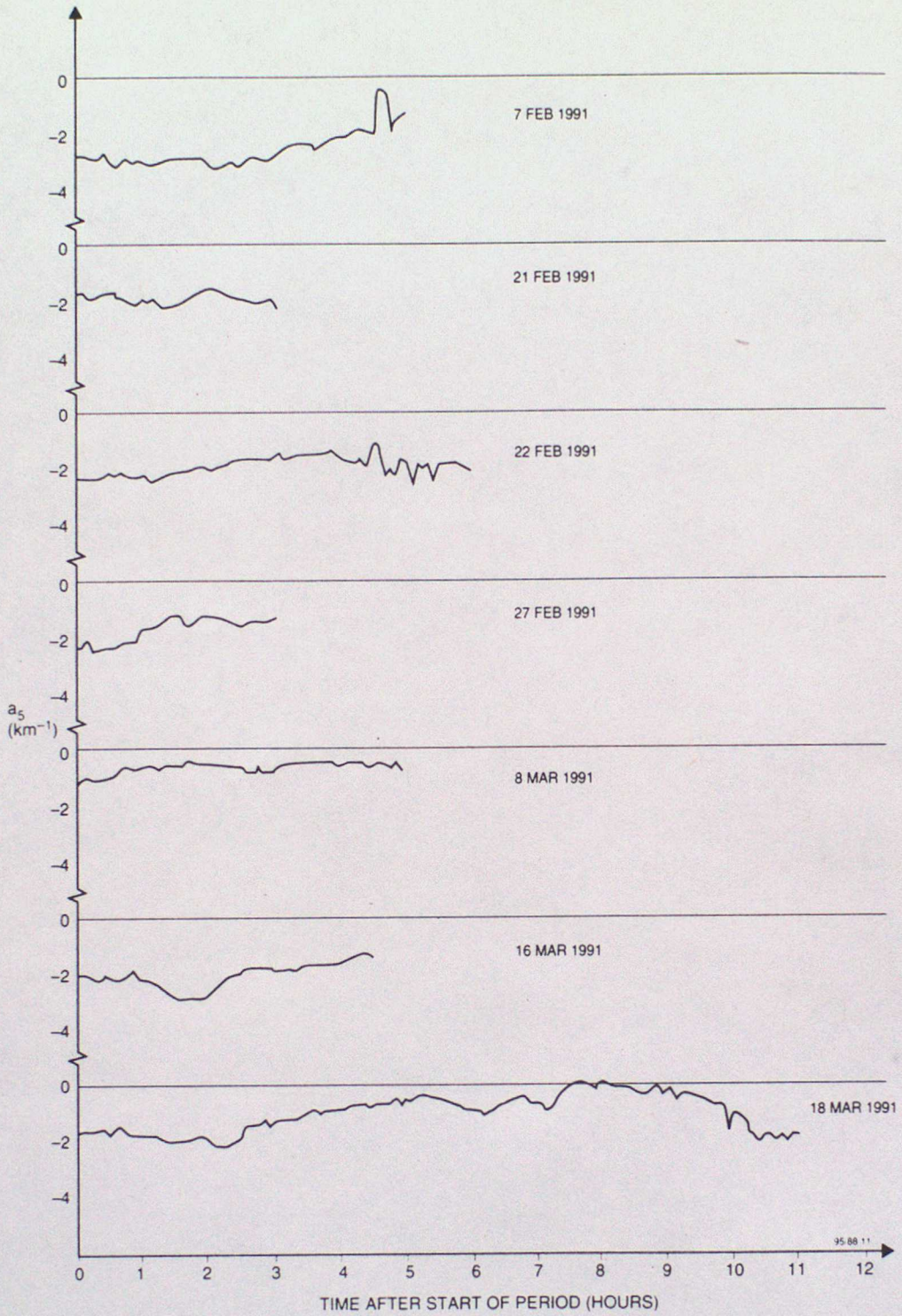

Fig 11. Similar to Fig 10 for analysis of data from the Wardon Hill radar in a further 7 randomly selected cases.